

An efficient fully nonlinear potential model for wave groups propagation over arbitrary bottoms

Xingya Feng^a, Qian Wu^{a,b*}

^aDepartment of Ocean Science & Eng, Southern University of Science and Technology, Shenzhen, China

^bDepartment of Civil & Environmental Eng, The Hong Kong Polytechnic University, Hong Kong, China

*qiann.wu@connect.polyu.hk

Highlights

- A fully nonlinear potential model is developed to simulate propagation of focused wave groups over a varying bathymetry.
- Second-order free waves and bound harmonics are decomposed from the nonlinear surface elevations.

1. Introduction

Understanding the underlying mechanisms of the generation of oceanic freak waves is important for forecasting and mitigating such natural disasters. One potential mechanism that has been investigated recently is nonlinear wave interaction with abrupt depth transitions (ADTs) (Li et al., 2021). Due to free surface nonlinearity, significant higher harmonics may be generated from wave-bottom interactions, increasing the probability of occurrence of large waves and wave resonances. The waves may be the superposition of components from reflection, dispersion by depth change and nonlinear wave-wave interaction, making it a complex wave system. An accurate nonlinear model is needed to capture all components. To investigate the nonlinear effect, separating the subharmonic and superharmonic components is also challenging. This work develops an efficient fully nonlinear potential flow model for simulating wave evolution over arbitrary bottoms. A conformal mapping method is employed to solve the two-dimensional boundary value problem. Focused wave groups are used as incoming waves. A submerged step is used to represent the ADTs. A four-phase manipulation technique by Feng et al. (2020) is implemented to decompose higher harmonics, and a Continuous Wavelet Transform (CWT) is employed to further decompose the higher bound (locked) and free waves. The spectral analysis and the separation techniques allow us to investigate the evolution of individual harmonics passing the submerged step in detail. Wave flume tests were carried out to validate the model.

2. Method

2.1. Experimental set-up

A rectangular step with a length of 2.4 m and a height of 0.24 m was submerged to form two water depth transitions, as shown in Fig. 1. The wave flume at the Hydrodynamic Laboratory at Southern University of Science and Technology is 20 meters long, 0.8 meters wide, and 1.2 meters deep. The water depth over the top of the step is 0.12 m, constituting one third of the incident water depth $h = 0.36$ m. Twenty capacitive wave gauges were placed along the x -axis in the same direction with wave propagation. A wave absorber located at the end of the wave flume is to minimize the reflected waves from the end. Focused wave groups were generated by a piston wavemaker. A phase manipulation approach was implemented to the wavemaker signals to prescribe the incident wave phases.

2.2. Mathematical formulation

A two-dimensional computational model is developed in this work to model wave propagating over varying bottoms using the conformal mapping method (Fig. 2). In the potential flow framework, the fluid is assumed to be incompressible, inviscid and the flow irrotational. The governing equations for the velocity potential $\phi(x, y, t)$ and the boundary conditions are as follows

$$\nabla^2 \phi = 0, \quad -h(x) < y < \eta(x), \quad (1)$$

$$\eta_t + \phi_x \eta_x - \phi_y = 0, \quad y = \eta(x), \quad (2)$$

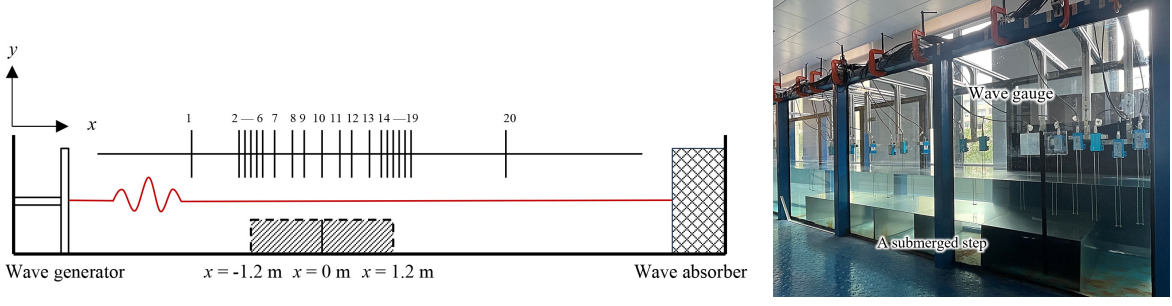


Figure 1: Sketch of the test setup and the snapshot.

$$\phi_t + \frac{1}{2} (\phi_x^2 + \phi_y^2) + g\eta = 0, \quad y = \eta(x), \quad (3)$$

$$\phi_y = 0, \quad y = -h(x), \quad (4)$$

where $\eta(x, y, t)$ is the surface elevation and g is the acceleration due to gravity. The subscript represents the derivative with respect to the variable. The bottom shape is described by a function $h(x)$, which can be arbitrary in the model.

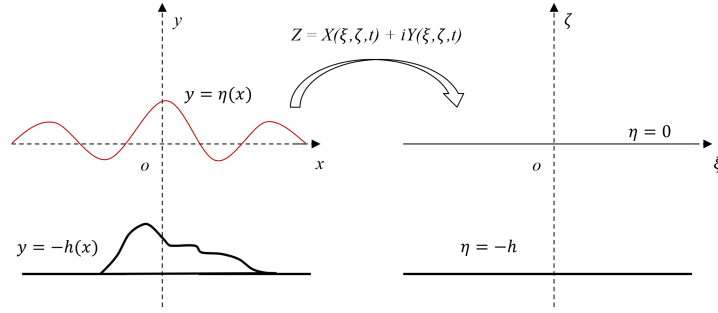


Figure 2: Transformation in the conformal mapping method.

A conformal mapping method is employed to solve the above problem. For the free surface and the bottom, a transformation is executed between the two domains: the physical domain and the mathematical domain. The physical plane (x, y, t) is mapped into the mathematical plane (ξ, ζ, t) using the complex analytic function $Z = X(\xi, \zeta, t) + iY(\xi, \zeta, t)$. The boundary value problem is solved in the mathematical plane, where the upper and lower boundaries are horizontal lines. The boundaries at the free surface $Y(\xi, 0, t)$ and the bottom $Y(\xi, -h, t)$ are expanded as a Fourier series in the mathematical domain

$$Y(\xi, 0, t) = \sum_{n=-\infty}^{n=\infty} \tilde{Y}_n e^{ink\xi}, \quad \zeta = 0, \quad (5)$$

$$Y(\xi, -h, t) = \sum_{n=-\infty}^{n=\infty} \tilde{B}_n e^{ink\xi}, \quad \zeta = -h, \quad (6)$$

where the Fourier coefficients of the bottom bathymetry and the free surface are denoted by \tilde{B}_n and \tilde{Y}_n , respectively. The numbers of Fourier terms are truncated based on the convergence. Using the Cauchy-Riemann relations $X_\xi = Y_\zeta$ and $X_\zeta = -Y_\xi$, we can easily obtain a new form of (X, Y) satisfying Eqs. (5) and (6). With the transformation of the boundary conditions in the two domains, the original governing equations in the physical domain can be described in the mathematical domain. The free surface and the bottom are transformed into two parallel lines, making it easy to solve the Laplace equation. The governing equations in the mathematical domain become

$$x_t - x_\xi \left\{ \tilde{h}_m \left[\frac{\psi_\xi}{J}, 0 \right] + q(t) \right\} - y_\xi \left(\frac{\psi_\xi}{J} \right) = 0, \quad (7)$$

$$y_t + x_\xi \left(\frac{\psi_\xi}{J} \right) - y_\xi \left\{ \tilde{h}_m \left[\frac{\psi_\xi}{J}, 0 \right] + q(t) \right\} = 0, \quad (8)$$

$$\phi_t + \frac{1}{J} \left\{ \frac{1}{2}(\phi_\xi^2 - \psi_\xi^2) - J\phi_\xi \tilde{h}_m \left[\frac{\psi_\xi}{J}, 0 \right] \right\} + gy = C(t), \quad (9)$$

where the Jacobian on the free surface is denoted by $J = x_\xi^2 + y_\xi^2$, and $C(t)$ is a time-dependent arbitrary function that can be incorporated into ϕ_t . $q(t)$ is defined as $q(t) = m \left\{ x_\xi \tilde{h}_m \left[\frac{\psi_\xi}{J}, 0 \right] + y_\xi \left(\frac{\psi_\xi}{J} \right) \right\}$, with \tilde{h}_m a Hilbert-transform-like operator. A pseudo-spectral method is used to discretize the free surface and the bottom boundaries by the Discrete Fourier Transform. In this study, the initial surface elevation and potential is prescribed based on the linear focused wave group model. A fixed-point iteration is used for time marching and to update the bathymetry $h(\xi, t)$ and the free surface in the simulation. Details on the computation can be found in Wu et al. (2024).

3. Results

A simple convergence study is firstly carried out to optimize the number of Fourier terms used for discretization of free surface and the bottom. Computational results show that over 50 terms or points per wavelength are sufficient to capture higher harmonic components up to fourth order. The computational results are then validated by the test results. A comparison of surface elevations for the test and the model in the temporal-spatial domain is shown in Fig. 3 at the selected gauges. A good between the measured and the computed is found. It is seen that the wave profiles at the designed focused positions $x = 7.7(-1.0)$ m become asymmetric with a sharper crest, presumably due to nonlinear effect.

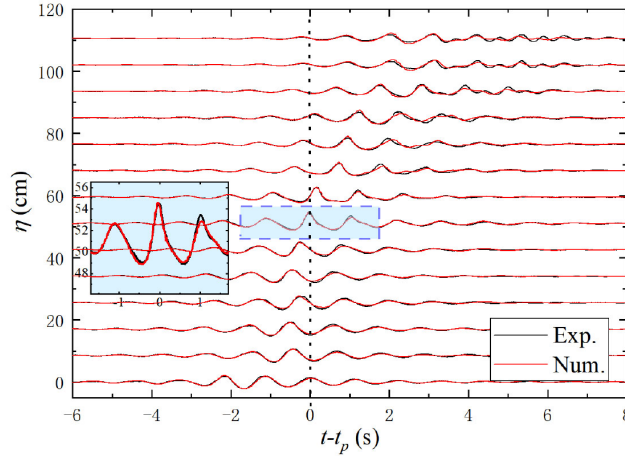


Figure 3: Surface elevations for the case $f_p = 0.9$ Hz.

Figure 4 displays the evolution of the amplitude spectrum for cases with two different peak frequencies $f_p = 0.8$ Hz and $f_p = 0.9$ Hz. The horizontal axis refers to the normalized frequency f/f_p . It is clear that the second harmonic component corresponding to the frequency range near $f/f_p = 2$ becomes significant at the first ADT $x = -1.2$ m. Third and higher harmonics can also be noticed on the step. This highlights the effect of higher harmonics potentially induced by the ADTs.

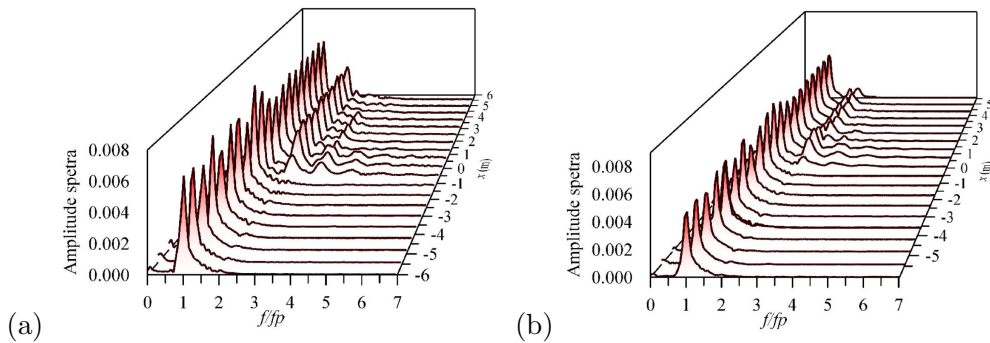


Figure 4: Spectral variation in space, (a) $f_p = 0.8$ Hz, $ka = 0.08$; (b) $f_p = 0.9$ Hz, $ka = 0.08$.

With the harmonic decomposition method using the phase manipulation, the second bound and free waves are difficult to be separated directly. The frequencies of the two components are both twice the fundamental harmonic. However, their wavenumbers are different because only the second free wave

satisfies the dispersion relation. Fig. 5 illustrates the distribution of wavenumbers of the focused wave groups in six time instants. It was found that the second bound wave with $2k_d$ was generated at the deeper water region before the group encountered the step. The second free waves $k_{sf}^{(2)}$ were induced when the wave group propagated over the first ADT at $t/T = 8.10$. With the Continuous Wavelet Transform (CWT) technique, the elevations of the second bound and free waves can be further separated. The results for the case $f_p = 1.0$ Hz are shown in Fig. 6 where the shaded area stands for the step. A sharp increase of the second bound waves at the first ADT is found. Then the second free wave is induced on the step which however is less significant than the bound one. The two components become comparable behind the step.

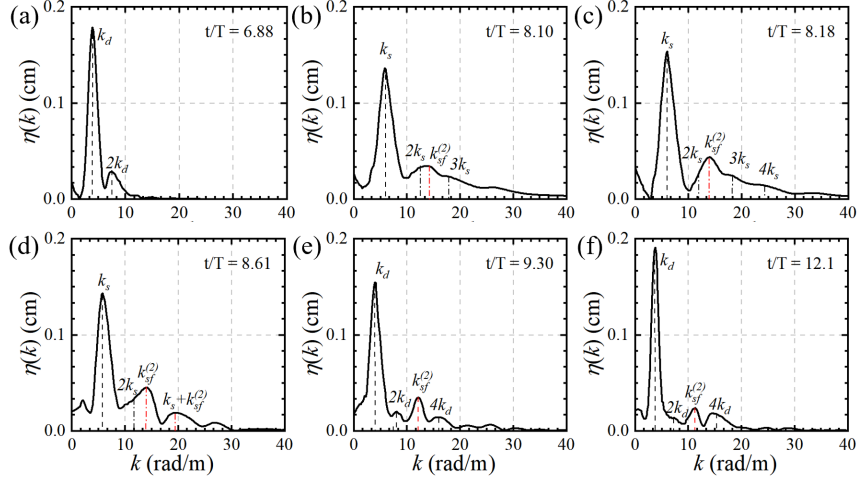


Figure 5: Distribution of wavenumber at different time moments for the case $f_p = 0.9$ Hz.

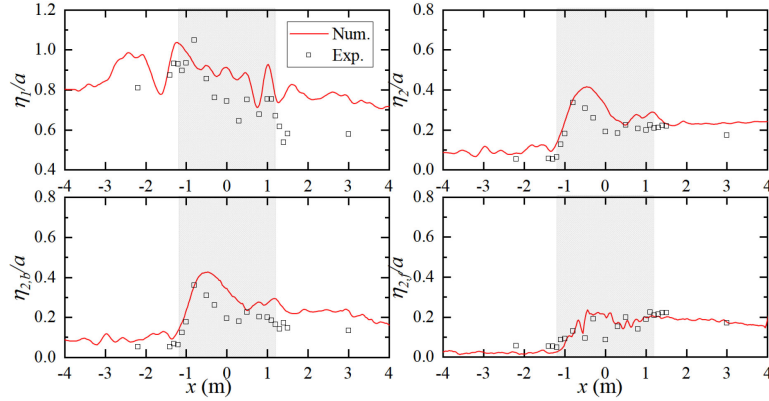


Figure 6: Distribution of amplitudes of second bound and free waves for the case $f_p = 1.0$ Hz.

4. Conclusions

The nonlinear propagation of focused waves over the ADTs is investigated numerically and experimentally. A fully nonlinear potential model is established utilizing the conformal mapping method. To capture the spectral evolution of higher harmonics, decomposition methods are employed to separate the superharmonics and the free waves. The existence of a submerged step causes an increase in the maximum amplitude and the higher harmonics. In the case of strong nonlinearity, higher order free waves become significant. The increase in the second harmonic at the second ADT is mainly due to the generation of free waves. The second bound wave reduces at the second ADT.

Feng, X., Taylor, P., Dai, S., Day, A., Willden, R., Adcock, T., 2020. Experimental investigation of higher harmonic wave loads and moments on a vertical cylinder by a phase-manipulation method. *Coastal Engineering* 160, 103747.

Li, Y., Zheng, Y., Lin, Z., Adcock, T.A., van den Bremer, T.S., 2021. Surface wavepackets subject to an abrupt depth change. part 1. second-order theory. *Journal of Fluid Mechanics* 915, A71.

Wu, Q., Feng, X., Dong, Y., 2024. Nonlinear bragg resonance of focused wave groups by periodic seabed topography. *Physics of Fluids* 36, 127131.